PCCP

ROYAL SOCIETY OF CHEMISTRY

PAPER

View Article Online
View Journal | View Issue

Cite this: *Phys. Chem. Chem. Phys.*, 2024, **26**, 15916

Separation of CO_2/CH_4 gas mixtures using nanoporous graphdiyne and boron-graphdiyne membranes: influence of the pore size†

Sahar Mahnaee, María J. López * and Julio A. Alonso

Nanoporous carbon-based membranes have garnered significant interest in gas separation processes owing to their distinct structure and properties. We have investigated the permeation and separation of the mixture of CO_2 and CH_4 gases through membranes formed by thin layers of porous graphdiyne (GDY) and boron graphdiyne (BGDY) using Density Functional Theory. The main goal is to investigate the effect of the pore size. The interaction of CO_2 and CH_4 with GDY and BGDY is weak, and this guarantees that those molecules will not be chemically trapped on the surface of the porous membranes. The permeation and separation of CO_2 and CH_4 through the membranes are significantly influenced by the size of the pores in the layers. The size of the hexagonal pores in BGDY is large in comparison to the size of the two molecules, and the passing of these molecules through the pores is easy because there is no barrier. Then, BGDY is not able to separate CO_2 and CH_4. In sharp contrast, the size of the triangular pores in GDY is smaller, comparable to the diameter of the two molecules, and this raises an activation barrier for the crossing of the molecules. The height of the barrier for CO_2 is one half of that for CH_4, the reason being that CO_2 is a linear molecule which adopts an orientation perpendicular to the GDY layer to cross the pores, while CH_4 has a spherical-like shape, and cannot profit from a favorable orientation. The calculated permeances favor the passing of CO_2 through the GDY membrane, and the calculated selectivity for CO_2/CH_4 mixtures is large. This makes GDY a very promising membrane material for the purification of commercial gases and for the capture of the CO_2 component in those gases.

Received 28th February 2024,
Accepted 22nd May 2024

DOI: 10.1039/d4cp00872c

rsc.li/pccp

1 Introduction

Greenhouse gas emissions related to human activity, particularly CO_2 emissions, have increased steadily over the past 100 years, contributing to global warming. This issue generates deep concern among citizens and many governments around the world. Indeed, reducing atmospheric CO_2 content is one of the most complex challenges facing modern society. Noteworthy, up to 80% of the world's energy demand is supplied by highly polluting fossil fuels. In spite of the commitment of international organizations, the pace of replacement of the contaminant energy sources by renewable clean energies is, by far, too slow to restrain global warming. Meanwhile, alternative strategies are being developed to reduce the excess of CO_2 in the atmosphere[1] and to contribute to reach the objective of carbon neutrality.

A promising strategy consists in the sequestration of CO_2, that is, the selective capture and storage of CO_2 in suitable sorbent materials. Post-combustion CO_2 capture is performed at the time of production, removing the CO_2 from the flue gases before its emission to the atmosphere. Pre-combustion capture separates CO_2 from CO_2/H_2 mixtures leading, ideally, to pure H_2 that can be used to generate energy. The purification of natural gas and landfill gas, and the biogas upgrading[2] through the separation of CO_2 from the CO_2/CH_4 mixtures, a process that improves their energy content, have acquired great relevance in the last years. A large variety of technologies and sorbents are being actively investigated[3,4] to improve the efficiency of more conventional sorbents based on zeolites and activated carbons. Among them, membrane-based technologies[5–7] offer many advantages, since they are easy to implement, scalable and energy efficient. The last years have witnessed significant developments on membranes for CO_2 capture and gas separation: MOF membranes,[8] carbon molecular sieve (CMS) membranes,[9] nanocomposite membranes,[10] ionic liquid (IL)-based membranes[11,12] and facilitated transport membranes (FTM).[13] In this context, nanomaterials show attractive characteristics.[4] Mazri *et al.* have

Departamento de Física Teórica, Atómica y Óptica, Universidad de Valladolid, 47011 Valladolid, Spain. E-mail: mariajlopez@uva.es

† Electronic supplementary information (ESI) available. See DOI: https://doi.org/10.1039/d4cp00872c

reviewed the application of graphene and graphene-based nanofluids for CO_2 absorption[4]

Gas separation is the central process on all these technologies. Therefore, abundant, cheap, recyclable filtering materials provide the key for the widespread use of these technologies. The two main factors for the efficient separation of gases are high permeability and selectivity of the membranes. Despite substantial advances, there is still a need to improve and develop novel membrane filtering materials to achieve a high selectivity towards one of the gases in the mixture without compromising their permeability.[7] It is known that the gas transport trough the filtering membrane is inversely proportional to its thickness. Therefore, since the discovery of graphene and the emergence of a large variety of 2-dimensional (2D) carbon based materials there has been great interest for the applicability of these 2D materials in filtration processes. These one atom-thick platforms bear a great potential for developing filtration membranes with excellent permeability. Thus, nanoporous graphene and graphene oxide (GO) membranes have been designed and proposed as efficient filters.[14–17] Molecular dynamics simulations demonstrate good performance of some arrays of these layers for CO_2/CH_4 separation. The main difficulty for developing these structures is the controlled generation of pores at the subnanometer level, with high precision on their size and position on the graphene layer. However, in recent years, members of a novel family of 2D carbon materials with a uniform distribution of pores of nanometric size and various shapes have been synthesized.[18,19] Graphynes are formed by hexagonal carbon rings, similar to those of graphene, but linked to each other through acetylenic chains of different lengths giving rise to triangular pores[18] or other shapes,[20] depending on the inserted linkages. It has been shown that doping these layers with heteroatoms (H, F, N) adds additional flexibility to improve/adjust the pore structure for the effective separation of gas mixtures.[21] The structure of another member of the family, boron graphdyine (BGDY), is imposed by the three-fold coordination of the boron atoms, linked by diacetylenic chains forming hexagonal pores.[19]

In this work, we examine and compare the utility of graphdiyne (GDY) and boron-graphdiyne (BGDY) layered nanostructures as membranes for the separation of gas mixtures. We expect that an array of these porous nanostructures can be helpful in gas separation technologies, and can achieve a high rate of gas throughput. Actually, GDY, and more in general graphynes, have been investigated for helium separation,[22] molecular hydrogen isotope separation,[23] hydrogen purification,[24–26] detection of dissolved gases in oil,[27] separation of oxygen from harmful gases,[28] separation of hydrogen from CO_2,[29] and separation of CO_2 from N_2.[30] The specific gas mixture that we study is the mixture of CH_4 and CO_2, of significant interest in biogas upgrading.[2,6] Different membrane materials have been investigated for the separation of this gas mixture: activated carbons,[31] mixed matrix membranes,[32,33] and hybrid organic–inorganic clay membranes.[34,35] We perform Density Functional calculations (DFT)[36] to investigate the performance of GDY and BGDY as membranes for the selective separation of CH_4 and CO_2 gas molecules. Specifically, as one of the main objectives of this work we study the important effect of the size of the pores on the permeability and selectivity of the membranes, since the pore sizes in GDY and BGDY are different. The theoretical method is briefly presented in Section 2, the results are reported in Section 3, and are discussed in Section 4. Finally, some conclusions are offered in Section 5.

2 Theoretical method

To perform the calculations, we have employed the Kohn–Sham DFT method[36] as implemented in the Quantum Espresso computational package.[37,38] The Perdew–Burke–Ernzerhof (PBE) generalized gradient (GGA) functional was used for electronic exchange–correlation effects.[39] The interaction between valence and core electrons was described by projector-augmented wave (PAW) pseudopotentials,[40,41] and dispersion interactions effects were included using Grimme's DFT-D3 method.[42,43] In a previous work by some of the authors[44] an extensive study of the interaction of molecular hydrogen with graphene and benzene was performed using DFT with a number of exchange–correlation functionals, and also several other quantum chemical methods. The conclusion was that the use of PBE with Grimme's semiempirical description of dispersion interactions gives accurate results for the interaction energy between H_2 and those substrates in comparison with more demanding quantum chemical methods. The nature of the chemical interaction of CO_2 and CH_4 with GDY and BGDY is just the same as that of H_2 with graphene, a weak interaction with an important van der Waals component, so the above conclusions also apply here. However, it is worth noticing that some differences exist between CO_2 (and CH_4) with respect to H_2. The main one in the present context arises from the electric dipole polarizabilities, which affect the dispersion interactions with the substrate: the measured polarizabilities of CO_2 and CH_4 are larger than that of H_2. The electronic wave functions are expanded in a basis of plane waves, with a cut-off energy of 45 Ry, and the cut-off for the electron density is 360 Ry. The Brillouin zone in reciprocal space was sampled with a $2 \times 2 \times 1$ Monkhorst–Pack grid.[45] The selected cut-off energies and grid of k points yield to a good convergence of the adsorption energies with a maximum numerical error of 2.0×10^{-4} eV (see Table S1 of the ESI†). The calculations were carried out in spin-polarized mode.

The main purpose of this work is to investigate the permeance of the CO_2 and CH_4 molecules through the hollow pores of the GDY and BGDY membranes. For this purpose, a key ingredient is to calculate the potential energy of the system as the molecule crosses from one side to the other side of the layer. Two types of paths have been considered. The first one is specified by the coordinates (0, 0, z), with varying z, of the centre of mass of the molecule; that is, the molecule follows a straight vertical path through the centre, placed at (0, 0, 0), of a specific pore of the membrane layer. In the second type of path, the x and y coordinates of the centre of mass of the molecule are allowed to relax to optimize the energy at each distance z from the layer. In all cases, that is, for both types of path, the

individual positions of the atoms of the membrane layers (GDY and BGDY), as well as the positions of the atoms of the molecules (CO_2 and CH_4) are fully relaxed at each step; that is, for each value of the distance z between the molecule and the layer.

3 Results

3.1 Structure of grapdiyne and boron-graphdiyne membranes

Graphdiyne[46,47] is a unique carbon allotrope that belongs to the family of graphyne. It is a two-dimensional layer material composed of carbon atoms arranged in a periodic hollow lattice structure shown in Fig. 1. In graphdiyne, some carbon atoms form hexagons, like in graphene. However, these hexagons are linked through carbon chains, resulting in a more complex structure showing large triangular holes. The distinctive feature of graphdiyne is the presence of both sp-hybridized and sp^2-hybridized carbon atoms. The sp^2-hybridized C atoms are those forming the hexagons, and the chains joining those aromatic ring hexagons are formed by sp-hybridized C atoms, leading to –C≡C–C≡C– chains with alternating triple (acetylenic) and single bonds. The calculated bond lengths along the carbon chains are: 1.39, 1.23, 1.33, 1.23, and 1.39 Å, and the carbon–carbon bond lengths in the carbon hexagons are larger, with an average value of 1.43 Å. These bond lengths agree well with previous work.[48] Because of the planar structure with triangular holes, GDY can be used as a membrane for the filtration of gases. The holes in the structure can also anchor metal clusters and the metal-functionalized GDY has been proposed as a promising material in catalysis and hydrogen storage.[48,49]

Boron graphdiyne, which has been synthesized by a bottom-up strategy,[19] is a two-dimensional layer material that contains boron and carbon atoms in its structure. The structure of BGDY, shown in Fig. 2, consists of a honeycomb lattice made up of hexagons, like in graphene. However, in BGDY the vertices of the hexagons are occupied by boron atoms, and chains of C atoms join those B atoms and form the sides of the large hexagonal holes. The C atoms in the structure of BGDY form diacetylenic chains, like the chains in GDY. The calculated B–C bond length is 1.52 Å, and the bond lengths of triple C≡C bonds and single C–C bonds are 1.23 Å and 1.36 Å, respectively, close to the values in GDY and in agreement with previous work.[49,50] The large hexagonal holes are a result of the boron atoms occupying the vertices of the hexagonal lattice. Because of the presence of these holes, the material can have applications in filtration membranes.

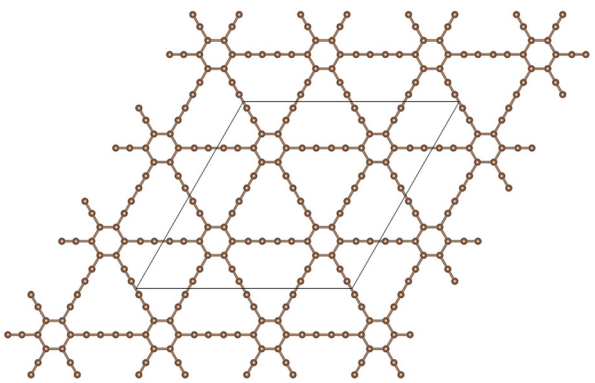

Fig. 1 Planar structure of graphdiyne, showing hexagonal rings linked by diacetylenic –C≡C–C≡C– chains, which form large triangular holes. The unit cell used in the calculations is highlighted.

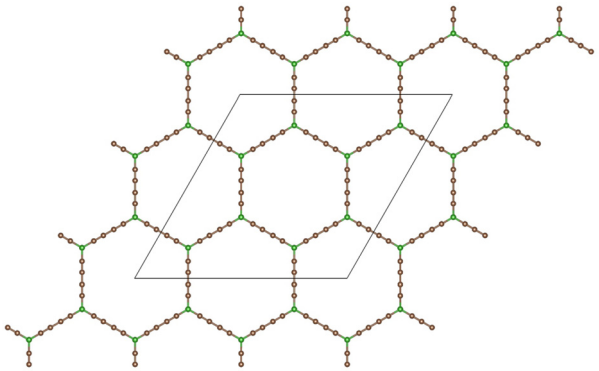

Fig. 2 Planar honeycomb structure of boron graphdiyne, showing hexagonal holes. BGDY is formed by boron atoms connected by carbon chains containing diacetylenic –C≡C–C≡C– linkages. Boron and carbon atoms are represented by green and brown spheres, respectively. The unit cell used in the calculations is highlighted.

3.2 Adsorption of CO_2 and CH_4 on the membrane surface

CO_2 is a linear molecule with calculated C–O bond distance of 1.20 Å. In methane, the four H atoms form a tetrahedron around a central C atom, and the calculated C–H bond distance is 1.09 Å. When the molecules of the gas mixture approach to the surface of the membrane, these molecules feel an attractive force due, at least, to the weak van der Waals interaction. But the force could be stronger if electrostatic or chemical interactions occur in addition. If the net attractive interaction is strong, the molecules will be trapped near the surface of the membrane, and passing through the membrane pores might be difficult. Of course, a barrier to cross the membrane may be present, as we discuss in the next section, and a deep interaction potential results in a high activation barrier. For this reason, it is important, as a first step, to know the strength of the adsorption energies of the molecules on the GDY and BGDY layers. The lowest energy adsorption configurations of one and several molecules (per hollow pore) on top of the GDY and BGDY layers were calculated, and the corresponding adsorption energies are reported in Table 1. The structures are given and described in the ESI.† The adsorption energy of a single CO_2 molecule is defined

$$E_{ads}(CO_2) = E(CO_2) + E(\text{layer}) - E(CO_2\text{-layer}), \quad (1)$$

written in terms of the energy of the system formed by the CO_2 molecule adsorbed on the substrate layer, and the energies of the isolated CO_2 molecule and substrate, and a similar equation holds for CH_4. The adsorption energies are small, and consequently there is no danger of the molecules being chemically trapped in those adsorption configurations under the

Table 1 Adsorption energies, in eV, for n CO_2 or n CH_4 molecules on GDY and BGDY. Adsorption energies per molecule are given in parentheses

	$n = 1$	$n = 2$	$n = 3$	$n = 4$
nCO_2/BGDY	0.121	0.272 (0.136)	0.429 (0.143)	0.614 (0.153)
nCH_4/BGDY	0.091	0.198 (0.099)	0.331 (0.110)	
nCO_2/GDY	0.168	0.333 (0.167)		
nCH_4/GDY	0.138	0.272 (0.136)		

usual filtration conditions. When n CO_2 molecules are adsorbed on top of the same hole of the substrate layer, the adsorption energy becomes

$$E_{ads}(nCO_2) = nE(CO_2) + E(\text{layer}) - E(nCO_2\text{-layer}), \quad (2)$$

with a similar equation for CH_4. The main difference between the BGY and BGDY substrates is that it becomes difficult to place a second molecule on top of the same hole of GDY, because the hole is small. In the case of CO_2 on GDY, the adsorption position of the second molecule is above a carbon chain, and adsorption on an adjacent triangular hole would be competitive. For CH_4 on GDY, the second molecule is displaced towards a vertex of the triangular hole. In contrast, when two or more molecules are adsorbed on the same hexagonal hole of BGDY, a weak cooperative effect is observed, in which the adsorption energy per molecule increases a bit with respect to the adsorption energy of a single molecule, because of the dispersive interaction between the adsorbed molecules.

Some results for mixed adsorption of nCO_2 and mCH_4 molecules are reported in Table 2. Total adsorption energies are compared with the sum $nE_{ads}(CO_2) + mE_{ads}(CH_4)$, where the values of those sums, calculated from the data in Table 1, are given in parentheses. Again, the effect of the attractive dispersion interaction between the molecules is observed. In summary, the strength of the interaction energies (per molecule) of CO_2 and CH_4 with GDY and BGDY is small, and will not prevent the passing of the molecules trough the hollow pores.

Further insight on the interaction between the CO_2 molecule and the GDY and BGDY layers is provided by the electron density redistribution taking place upon adsorption of CO_2 on those supporting layers, defined as

$$\Delta\rho(\vec{r}) = \rho_{CO_2\text{-layer}}(\vec{r}) - \rho_{\text{layer}}(\vec{r}) - \rho_{CO_2}(\vec{r}) \quad (3)$$

where $\rho_{CO_2\text{-layer}}(\vec{r})$ is the electron density of the system formed by the CO_2 molecule adsorbed on the GDY (or BGDY) layer, and $\rho_{\text{layer}}(\vec{r})$ and $\rho_{CO_2}(\vec{r})$ are the densities of the separated GDY (or BGDY) layer and CO_2 molecule, where the separated subsystems hold the same structure as in the adsorbed system. A similar definition applies to CH_4 adsorption on GDY and BGDY. The electron density redistributions are shown in Fig. 3. The figure

Table 2 Adsorption energies, in eV, for nCO_2 plus mCH_4 molecules on BGDY. The values in parentheses represent the sum $nE_{ads}(CO_2) + mE_{ads}(CH_4)$

	$n = 1, m = 1$	$n = 2, m = 3$
Adsorption energy	0.244 (0.212)	0.695 (0.515)

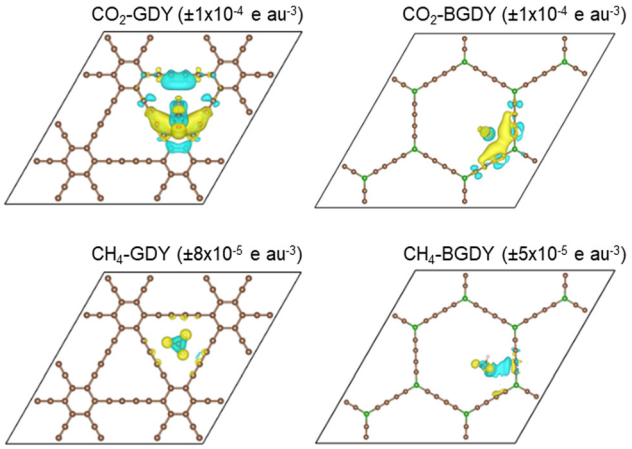

Fig. 3 Electron density redistribution $\Delta\rho(\vec{r})$ for the adsorption of CO_2 (upper panels) and CH_4 (lower panels) on the GDY and BGDY layers. Isodensity surfaces with positive (in yellow) and negative (in blue) values of $\Delta\rho$ are represented. The values of $\Delta\rho$ are indicated in parenthesis in the figure for each molecule-layer system. Positive (negative) values of $\Delta\rho$ correspond to regions where the electron density increases (decreases) in the adsorbed molecule-layer system with respect to the superposition of the densities of the separated subsystems.

shows that the density redistribution is small in all cases. One can observe a tiny accumulation of electronic charge between the CO_2 molecule and the two diacetylenic chains of GDY (or BGDY) closer to the molecule (notice the small value of the $\Delta\rho$ isodensity surface plotted) and a tiny polarization of the electron density in the CH_4 molecule. The density redistribution concentrates mainly on the adsorbed CO_2 or CH_4 molecules, and the GDY and BGDY substrates are mostly unaffected. The electron density redistribution confirms the weak interaction (van der Waals type) between CO_2 and CH_4 molecules and GDY and BGDY layers, and the absence of electrostatic or chemical interactions between the molecules and the supporting layers that would impede the passing of the molecules through the pores of the layers.

We are not aware of other works for the interaction of CO_2 and CH_4 with GDY or BGDY. But some information exists for the interaction of these molecules with other related carbon materials. DFT calculations of the adsorption energies of CO_2 and CH_4 with graphene have been performed.[51–53] The adsorption energies of CO_2 on graphene calculated by Wood *et al.*[52] and Thierfelder *et al.*[53] vary between 0.12 and 0.16 eV per molecule, depending on the exchange–correlation energy functional used, and the treatment of dispersion. These results are in good agreement with the experimental value of 0.127 eV per molecule. The calculated adsorption energy of CH_4 is 0.24 eV per molecule.[52] The adsorption energies obtained by Ossouledini *et al.*[51] are smaller, 0.03 eV per molecule (CO_2) and 0.05 eV per molecule (CH_4). Overall, these results are consistent with the results in Table 1. All the adsorption energies reveal the fact that the attractive part of the interaction of CO_2 and CH_4 with the three planar substrates, graphene, GDY and BGDY, is weak, dominated by dispersion effects, although differences can be expected between the difference substrates. Ganji[54] investigated

the interaction of CO_2 with carbon nanotubes using DFT, and obtained an adsorption energy of 0.38 eV per molecule. This energy is larger than the adsorption energies quoted above, and this can be understood as due to the higher reactivity of the curved nanotubes.

3.3 Vertical path of CO_2 and CH_4 through the center of the pores of GDY and BGDY

We now investigate the filtration of CO_2 and CH_4 through the GDY and BGDY membranes. The passing of these molecules through the hollow pores of GDY and BGDY has been first simulated by placing the molecules at a distance z above the center of a hollow pore, that is, fixing the (x, y, z) coordinates of the C atom of those molecules at $(0, 0, z)$, and calculating the energy of the whole system, molecule and membrane layer, for several different distances z of approach (these conditions will be relaxed in Section 3.4). For each value of z, the orientation of the molecules, and also the interatomic distances in the molecule, and the coordinates of the atoms of the membranes are fully relaxed to optimize the energies. In this way, the potential energy of the molecule along a path (with $x = y = 0$) approaching the layer is obtained.

The energy *versus* distance z is plotted in Fig. 4. The main difference between the GDY and BGDY membranes is that the strength of the interaction between these molecules and BGDY is substantially lower than their interaction with GDY. This is due to the larger size of the holes in BGDY. The minimum of the potential energy curves occurs near $z = 2$–3 Å in GDY, and at $z = 0$ in BGDY. This means that there is an activation barrier for the passing of CO_2 and CH_4 through the triangular holes of GDY (notice that the potential energy curve is symmetrical with respect to the layer plane). The magnitude of the barrier is quite different: 0.28 eV for CO_2, and 0.51 eV for CH_4. On the other hand, the passing of the two molecules through the hexagonal holes of BGDY is much easier: the depth of the minimum at $z = 0$ is tiny, with values of -0.029 for CO_2, and -0.030 eV for CH_4, and there are no barriers for the passing from one side of the membrane layer to the other.

The particular orientation of the molecular axis of the linear CO_2 molecule is not relevant when the molecule is far away, or at least not close to the GDY layer. At distances z near the potential energy minimum, the orientation of the CO_2 axis is a bit tilted with respect to the plane of the GDY layer; see Fig. 5. However, the orientation becomes perpendicular when the molecule approaches closely the layer. This reorientation of the molecular axis occurs spontaneously in the calculations, because it lowers the short-range Pauli repulsion with the pore walls and facilitates the crossing of the molecule through the narrow hole. The vertical orientation of the axis can be interpreted as a way of decreasing the effective size of the CO_2 molecule, as sensed by the pore boundaries, in comparison to other molecular orientations, when passing through the hole. On the other hand, the shape of CH_4 is nearly spherical, and its orientation is not relevant. The boundaries of the hole deform slightly through the crossing of CH_4, but not through the crossing of CO_2 (due to the favorable orientation). The boundaries of the large hexagonal holes of BGDY do not suffer deformation through the passing of CO_2 or CH_4, as shown in Fig. 6.

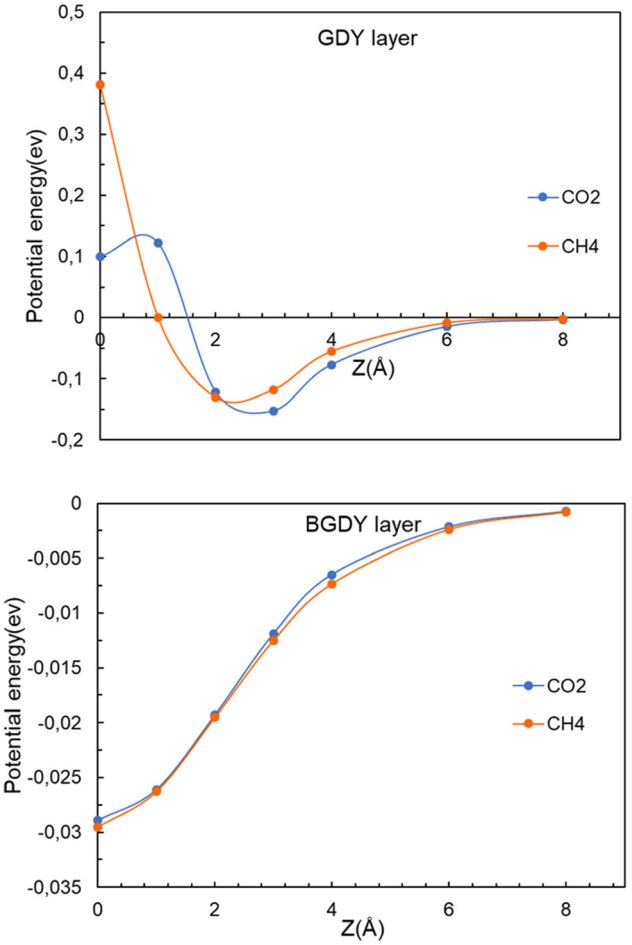

Fig. 4 Energy as a function of the distance z between the CO_2 or CH_4 molecules and the layer. Upper panel, GDY. Lower panel, BGDY. The (x, y) coordinates of the molecule are $x = 0$, $y = 0$.

To clarify the nature of the interaction between these molecules and the GDY and BGDY layers, the interaction energy and its attractive van der Waals contribution are plotted in Fig. 7 for the case of CO_2 interacting with GDY. The two curves are very close until the molecule approaches the layer at a distance of 3 Å. However, as the molecule approaches closer to the layer, the total interaction turns repulsive because the molecule does not fit well into the triangular hole due to the short-range repulsive interaction with the pore walls, and some energy has to be invested to go through.

3.4 Relaxation of the crossing path

The straight vertical path $(0, 0, z)$ through the center of the hollow pores serves to illustrate well the form of the potential energy of interaction (see Fig. 4). However, in their travel the molecules might deviate from the $(0, 0, z)$ vertical path if this lowers the potential energy. New calculations have been performed by allowing for those deviations. That is, at each specific value of the z coordinate of the center of mass of the

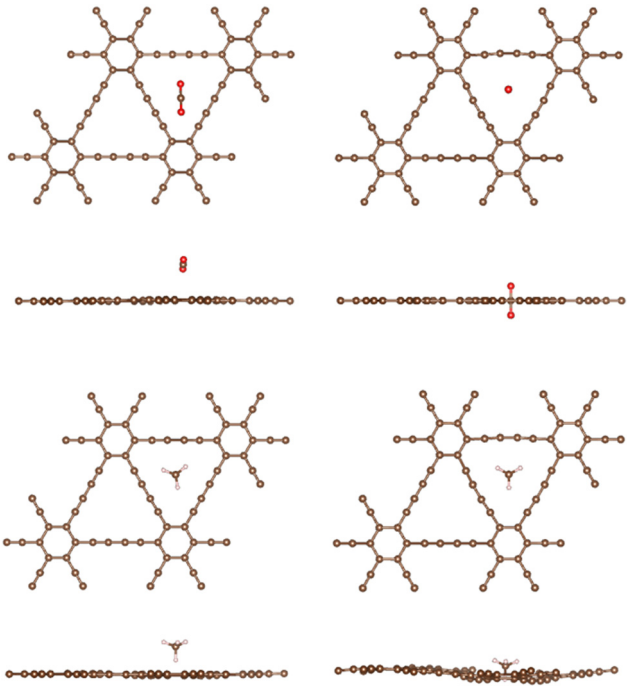

Fig. 5 Top and lateral views of the orientation of the CO_2 molecule on GDY, at z = 3 Å, and z = 0. Same for CH_4 at z = 2 Å, and z = 0. The calculations assume $x = y = 0$. Oxygen, carbon and hydrogen atoms are represented by red, brown, and light grey spheres, respectively.

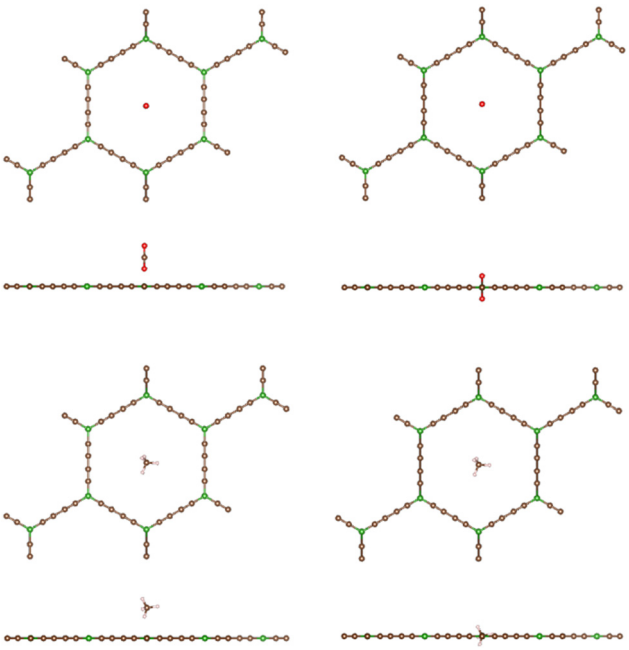

Fig. 6 Top and lateral views of the orientation of the CO_2 molecule at z = 3 Å, and on the plane of the BGDY layer, z = 0 Å. Same for CH_4. The calculations assume $x = y = 0$. Oxygen, carbon and hydrogen atoms are represented by red, brown, and light grey spheres, respectively.

molecule (vertical distance to the layer) the x and y coordinates of the center of mass were allowed to relax to optimize the

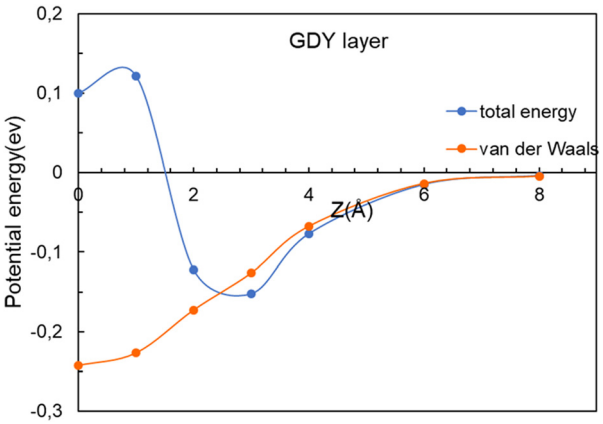

Fig. 7 Energy as a function of the distance z between the CO_2 molecule and the GDY layer. The (x, y) coordinates of the molecule are x = 0, y = 0. The van der Waals contribution is also included.

energy, in addition to the full relaxation of the orientation and interatomic distances of the molecule and the positions of all the atoms of the membrane. The improved interaction potentials for the passing of CO_2 and CH_4 through the GDY pores are plotted in Fig. 8. By comparison with Fig. 4, no appreciable changes are observed in the potential energies of the two molecules. The positions of the energy minima and the magnitude of the activation barriers are practically the same as in Fig. 4. The position and orientation of the molecules near the potential energy minimum, and at z = 0 are practically indistinguishable from those in Fig. 5; that is, the deviation of the path of the molecules from the path with $x = y = 0$ is negligible. The main conclusion from Fig. 4 and 8, is that the different heights of the barriers for CO_2 and CH_4 reveal the excellent selectivity of the GDY:CO_2 molecules will pass much more easily than CH_4 molecules through the triangular holes. And one can profit from this fact to purify commercial gas, and to capture the CO_2.

In sharp contrast, in the case of BGDY, with large hexagonal pore holes, the relaxation of the (x, y) coordinates of the

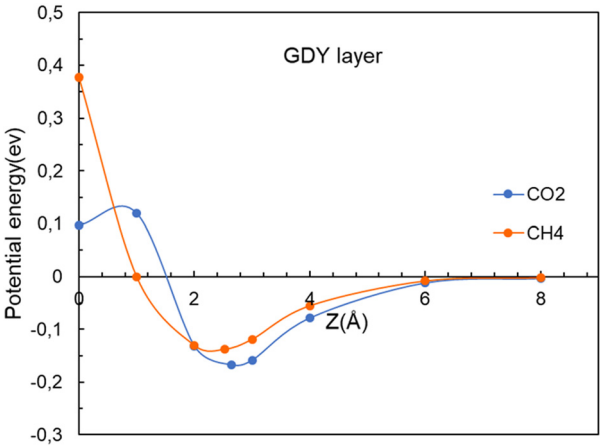

Fig. 8 Energy as a function of the distance z between the CO_2 and CH_4 molecules and the GDY layer. The (x, y) coordinates of the molecules are relaxed for each value of z.

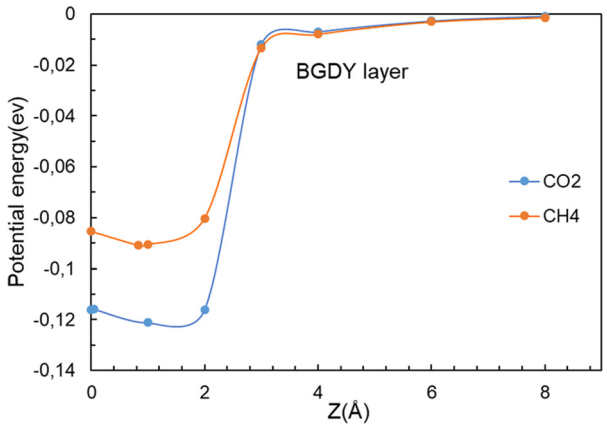

Fig. 9 Energy as a function of the distance z between the CO_2 and CH_4 molecules and the BGDY layer. The (x, y) coordinates of the molecules are relaxed for each value of the vertical distance z.

molecules affects substantially their potential energies. Fig. 9 shows that the minima of the potential energy curves become deeper in comparison to Fig. 4, because the path of the molecules moves a bit towards one corner of the hexagon (see Fig. 10), in this way increasing the attractive van der Waals interaction with the layer. The barriers for the crossing of CO_2 and CH_4 molecules from one side of the BGDY layer to the other through the hexagonal holes are negligibly small, and the depth of the potential confining the molecules in the region close to the layer is small in both cases, and easily surmountable under the usual filtration conditions. This means that BGDY is much less effective to separate CO_2 and CH_4.

4 Discussion

The potential energy minima at distances of 2–3 Å from the GDY layer shown in Fig. 8 indicate that there is a stable adsorption configuration for CO_2 and CH_4 when these molecules are close to the GDY layer. This is mainly due to the attractive van der Waals interactions between the molecules and the GDY, and the depths of the minima are small. The barrier to go through the hollow cavities arises because the sizes of these molecules and the size of the pores are relatively similar. However, the barrier for CO_2 is smaller than the barrier for CH_4, because CO_2 is a linear molecule that can adopt a favorable orientation, perpendicular to the layer, to cross the holes. On the other hand, CH_4 is nearly spherical and cannot profit from a favorable orientation. Fig. 11 shows the electronic densities of CO_2 and CH_4 at the point of passing through the GDY membrane, that is, at $z = 0$. At this point, the axis of the CO_2 molecule is, as mentioned above, perpendicular to the GDY layer. Surfaces of constant density with a value 0.01 e a.u.$^{-3}$ have been plotted, and these reflect well the difference in size of the two molecules that permits the easier crossing of CO_2 through the triangular hole.

The energy barriers are critical for controlling the permeation of molecules through the material. Smaller activation barriers indicate that it is easier for those molecules to pass

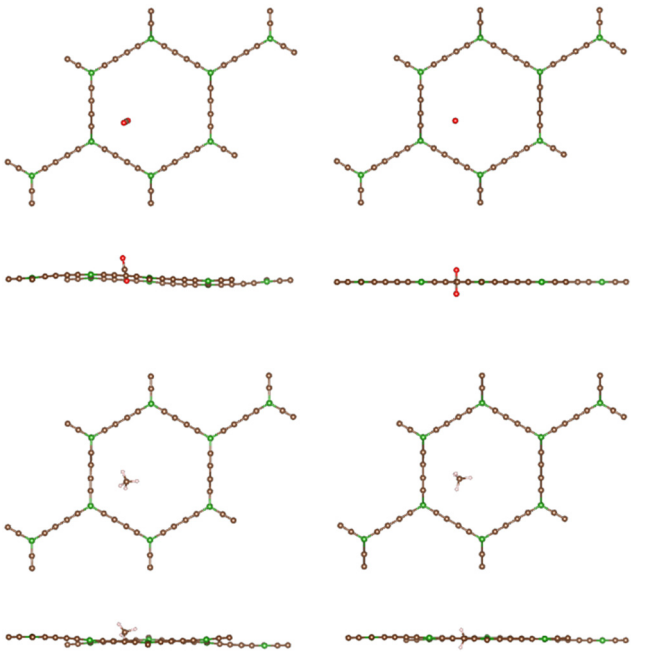

Fig. 10 Top and lateral views of the orientation of the CO_2 and CH_4 molecules on BGDY, at $z = 1$ Å, and $z = 0$. Oxygen, carbon and hydrogen atoms are represented by red, brown, and light grey spheres, respectively. The (x, y) coordinates of the center of mass of the molecules are relaxed for each value of z.

through. This property can be exploited to create selective membranes allowing certain molecules to pass, while inhibiting others. In our case, GDY membranes will be able to separate a mixture of CO_2 and CH_4, allowing the purification of natural gas and biogas, as well as the capture of the CO_2.

The relative sizes of the pores and gas molecules are the major factor determining what molecules can pass easily through the membrane. The sizes of CO_2 and CH_4 are quite similar, the experimental bond-lengths being d(C–O) = 1.16 Å, and d(C–H) = 1.09 Å. But CO_2 is a linear molecule, and by adopting the vertical orientation with respect to the membrane layer, its effective size when passing through the hollow pore is much reduced.

The size of the hexagonal pores in BGDY is substantially larger than the sizes of CO_2 and CH_4, and these molecules will easily pass through the layer holes. The molecules have a tendency to deviate from the $x = y = 0$ path, a fact that increases the attractive part of the interaction with the BGDY layer, but

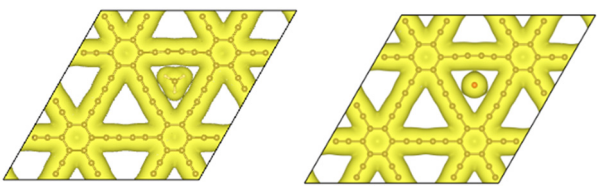

Fig. 11 Top view of the electronic density of CH_4 (left panel) and CO_2 (right panel) at the point of passing through the GDY membrane, $z = 0$. The yellow regions correspond to a surface of constant electron density with the value 0.01 e a.u.$^{-3}$.

the passing through the hollow pores is still easy because there is no activation barrier. BGDY will not serve to separate CO_2 and CH_4, but could serve to separate CO_2 and CH_4 from larger molecules, like large hydrocarbons.

To quantitatively assess the capacity of GDY to separate CO_2 and CH_4, the selectivity of the membrane and the permeances of the two gases can be calculated. The selectivity of the GDY membrane to separate CO_2 and CH_4 can be obtained by starting from Arrhenius equation

$$A = A_0 e^{-E_b/k_B T} \quad (4)$$

where A is the diffusion rate, A_0 is a diffusion prefactor, E_b is the diffusion barrier, k_B is the Boltzmann constant, and T is the temperature. A good approximation is to assume that the diffusion prefactors are equal for CO_2 and CH_4.[28,29,55,56] Then, the selectivity S is obtained as

$$S(CO_2/CH_4) = \frac{A(CO_2)}{A(CH_4)} = e^{-(E_b(CO_2)-E_b(CH_4))/k_B T}. \quad (5)$$

The selectivity as a function of the temperature is shown in Fig. 12 (the actual values are given in Table S2 of the ESI†). Evidently, the selectivity decreases with increasing temperature. But at room or lower temperatures the selectivity is substantial and promising, reaching a value near 10^4 at room temperature, which guarantees an efficient separation of the two gases, and the capture of the CO_2 component. Selectivities of this order have been obtained in works for other gas mixtures.[28,29]

The permeance of a membrane for a gas[28] is defined by

$$P = F/\Delta p. \quad (6)$$

In this equation, F is the gas molar flux through the membrane, and Δp the pressure difference between the two sides of the membrane. F is calculated as $F = Nf$, where N represents the number of gas molecules per unit surface and unit time colliding with the membrane, and f is the probability for a particle to diffuse through the pore at a given velocity. The kinetic theory of gases allows to write N as

$$N = \frac{p}{\sqrt{2\pi MRT}}, \quad (7)$$

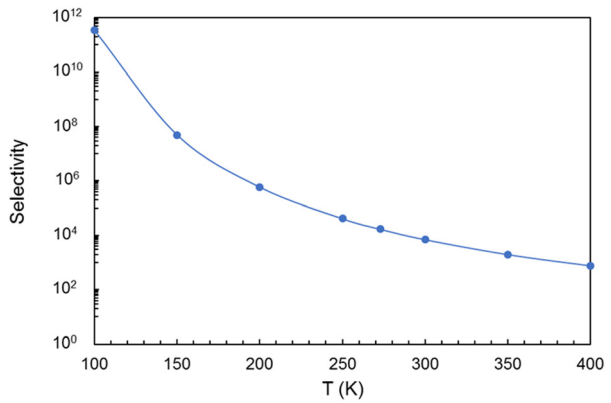

Fig. 12 Selectivity $S(CO_2/CH_4)$ of the GDY membrane for different temperatures.

with M, R and T standing for the molar mass, the gas constant and the temperature. Next, the probability f is calculated from the Maxwell–Boltzmann velocity distribution

$$f(v)d^3v = \left(\frac{m}{2\pi k_B T}\right)^{3/2} e^{-\frac{m\left(v_x^2+v_y^2+v_z^2\right)}{2k_B T}} dv_x dv_y dv_z \quad (8)$$

where m is the mass of the molecule. The probability f is the integral of that distribution over the velocities of the gas molecules under the constraint that v_z is larger than v_b, where v_b stands for the velocity leading to a kinetic energy equal to the height of the diffusion energy barrier. Then the integral will involve exclusively those gas molecules having kinetic energies high enough to overcome the diffusion barrier. Integrating over the x and y components of the velocity, the Maxwell–Boltzmann distribution for the z direction becomes

$$f(v_z)dv_z = \left(\frac{m}{2\pi k_B T}\right)^{1/2} e^{-\frac{mv_z^2}{2k_B T}} dv_z. \quad (9)$$

Therefore, the probability f is given by

$$f = \int_{v_b}^{\infty} f(v_z)dv_z. \quad (10)$$

Taking into account the properties of the Gaussian integral,[57] f becomes

$$f = \frac{1}{2} - \int_0^{v_b} f(v_z)dv_z, \quad (11)$$

which can be expressed in terms of the error function

$$f = \frac{1}{2}\left[1 - \mathrm{erf}\left(\left(\frac{m}{2k_B T}\right)^{1/2} v_b\right)\right]. \quad (12)$$

The calculated permeances of CO_2 and CH_4 through GDY are plotted in Fig. 13 as a function of the temperature, for an incoming pressure $p = 3 \times 10^5$ Pa and a pressure difference between the two sides of the membrane $\Delta p = 10^5$ Pa. The permeance of CO_2 is higher than the permeance of CH_4, which is consistent with the calculated selectivity of GDY. The horizontal line plotted in this Figure marks the industrial permeance limit for gas separation processes, which is 6.7×10^{-9} mol m^{-2} s^{-1} Pa^{-1}. These results confirm that GDY can act as a porous membrane for the effective separation of CO_2 and CH_4, and for the capture of the CO_2 in the natural gas industry.

5 Conclusions

The capacity of GDY and BGDY nanoporous membranes to separate CO_2 and CH_4 in a CO_2/CH_4 gas mixture has been investigated. This process is relevant in the purification of natural gas, landfill gas, and biogas. The strength of the interaction between these two molecules and GDY or BGDY is small. Consequently, these molecules are not chemically bound to the membrane layers, and passing through the holes of the GDY and BGDY membranes is possible under the usual filtration conditions. A crucial difference between the two membranes is that the size of the hexagonal pores in BGDY is large

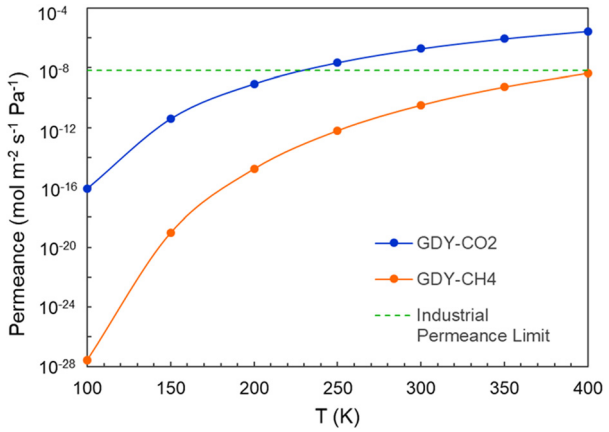

Fig. 13 Permeance of CO_2 and CH_4 through GDY as a function of temperature for an incoming pressure $p = 3 \times 10^5$ Pa and a pressure difference between the two sides of the membrane $\Delta p = 10^5$ Pa. The horizontal line represents the industrial permeance limit.

in comparison to the size of the two molecules, and the crossing of these molecules through the pores of BGDY is easy because of the lack of activation barriers. Then, BGDY is not efficient to separate CO_2 and CH_4. On the other hand, the size of the triangular pores in GDY is smaller, comparable to the diameters of the two molecules, and this builds up an activation barrier for the passing of the molecules. The height of the barrier for CO_2 is approximately one half of that for CH_4. The reason is that CO_2 is a linear molecule which adopts an orientation perpendicular to the GDY layer to cross the pores, in this way reducing its effective size during the crossing process. In contrast, CH_4 has a spherical-like shape, and cannot profit from a favorable orientation. For these reasons, the calculated selectivity of the GDY membrane for CO_2/CH_4 separation is large, and favors the passing of CO_2. The calculated permeances are consistent with the selectivity. This makes GDY a very promising membrane material for the purification of commercial gas and for the capture of its CO_2 component.

Author contributions

Sahar Mahnaee: conceptualization; formal analysis; investigation; writing – original draft; visualization. María J. López: conceptualization; formal analysis; investigation; writing – review & editing; supervision; funding acquisition. Julio A. Alonso: conceptualization; formal analysis; investigation; writing – original draft; writing – review & editing; supervision.

Conflicts of interest

There are no conflicts to declare.

Acknowledgements

Work supported by Ministerio de Ciencia e Innovación of Spain (grants PID2019-104924RB-I00 funded by MCIN/AEI/10.13039/501100011033, and PID2022-138340OB-I00 funded by MCIN/AEI/10.13039/501100011033 and FSE+), and the University of Valladolid (GIR Nanostructure Physics Group). S. M. acknowledges a predoctoral contract with the University of Valladolid.

References

1 *Carbon capture, storage and utilization: a possible climate change solution for energy industry*, ed. M. Goel, M. Sudhakar, and R. V. Sahi, CRC Press, 2019.
2 X. Yuan Chen, H. Vinh-Thang, A. Avalos Ramirez, D. Rodrigue and S. Kaliaguine, Membrane gas separation technologies for biogas upgrading, *RSC Adv.*, 2015, **5**, 24399–24448, DOI: **10.1039/C5RA00666J**.
3 A. Alonso, J. Moral-Vico, A. Abo Markeb, M. Busquets-Fité, D. Komilis, V. Puntes, A. Sánchez and X. Font, Critical review of existing nanomaterial adsorbents to capture carbon dioxide and methane, *Sci. Total Environ.*, 2017, **595**, 51–62, DOI: **10.1016/j.scitotenv.2017.03.229**.
4 N. Azni Farhana Mazria, A. Arifutzzamana, M. Kheireddine Arouaa, M. Ekhlasur Rahmand and S. Ali Mazari, Graphene and its tailoring as emerging 2D nanomaterials in efficient CO_2 absorption: A state-of-the-art interpretative review, *Alexandria Eng. J.*, 2023, **77**, 479–502, DOI: **10.1016/j.aej.2023.06.070**.
5 A. G. Olabi, A. H. Alami, M. Ayoub, H. Aljaghoub, S. Alasad, A. Inayat, M. A. Abdelkareem, K.-J. Chae and E. T. Sayed, Membrane-based carbon capture: Recent progress, challenges, and their role in achieving the sustainable development goals, *Chemosphere*, 2023, **320**, 137996, DOI: **10.1016/j.chemosphere.2023.137996**.
6 F. M. Baena-Moreno, E. le Saché, L. Pastor-Pérez and T. R. Reina, Membrane-based technologies for biogas upgrading: a review, *Environ. Chem. Lett.*, 2020, **18**, 1649–1658, DOI: **10.1007/s10311-020-01036-3**.
7 M. Farnam, Hilmi bin Mukhtar and Azmi bin Mohd Shariff, A Review on Glassy and Rubbery Polymeric Membranes for Natural Gas Purification, *ChemBioEng Rev.*, 2021, **8**(2), 90–109, DOI: **10.1002/cben.202100002**.
8 H. Demir, G. O. Aksu, H. C. Gulbalkan and S. Keskin, MOF Membranes for CO_2 Capture: Past, Present and Future, *Carbon Capture Sci. Technol.*, 2022, **2**, 100026.
9 W. Li, K. Goh, C. Y. Chuah and T.-H. Bae, Mixed-matrix carbon molecular sieve membranes using hierarchical zeolite: A simple approach towards high CO_2 permeability enhancements, *J. Membr. Sci.*, 2019, **588**, 117220.
10 D. Chen, K. Wang, Z. Yuan, Z. Lin, M. Zhang, Y. Li, J. Tang, Z. Liang, Y. Li, L. Chen, L. Li, X. Huang, S. Pan, Z. Zhu, Z. Hong and X. He, Boosting membranes for CO_2 capture toward industrial decarbonization, *Carbon Capture Sci. Technol.*, 2023, **7**, 100117.
11 A. R. Nabais, S. Ahmed, M. Younis, J.-X. Zhou, J. R. Pereira, F. Freitas, D. Mecerreyes, J. G. Crespo, M. H. Huang and L. A. Neves, *et al.*, Mixed matrix membranes based on ionic liquids and porous organic polymers for selective CO_2 separation, *J. Membr. Sci.*, 2022, **660**, 120841.

12 N. N. R. Ahmad, C. P. Leo and A. W. Mohammad, Enhancement on the CO_2 separation performance of mixed matrix membrane using ionic liquid, *Mater. Lett.*, 2021, **304**, 130736.
13 H. Guo, J. Wei, Y. Ma, J. Deng, S. Yi, B. Wang, L. Deng, X. Jiang and Z. Dai, Facilitated transport membranes for CO_2/CH_4 separation—State of the art, *Adv. Membr.*, 2022, **2**, 100040.
14 S. Blankenburg, M. Bieri, R. Fasel, K. Müllen, C. A. Pignedoli and D. Passerone, Porous graphene as an atmospheric nanofilter, *Small*, 2010, **6**, 2266e71.
15 H. W. Kim, H. W. Yoon, S.-M. Yoon, B. M. Yoo, B. K. Ahn, Y. H. Cho, H. J. Shin, H. Yang, U. Paik, S. Kwon, J.-Y. Choi and H. B. Park, Selective Gas Transport Through Few-Layered Graphene and Graphene Oxide Membranes, *Science*, 2013, **342**, 91, DOI: **10.1126/science.1236098**.
16 N. Razmara, A. Kirch, J. Romano Meneghini and C. Rodrigues Miranda, Efficient CH_4/CO_2 gas mixture separation through nanoporous graphene membrane designs, *Energies*, 2021, **14**, 2488, DOI: **10.3390/en14092488**.
17 A. Ali, M. Aamir, K. H. Thebo and J. Akhtar, Laminar graphene oxide membranes towards selective ionic and molecular separations: Challenges and progress, *Chem. Rec.*, 2019, **19**, 1–12, DOI: **10.1002/tcr.201900024**.
18 G. Li, Y. Li, H. Liu, Y. Guo, Y. Lia and D. Zhu, Architecture of graphdiyne nanoscale films, *Chem. Commun.*, 2010, **46**, 3256–3258, DOI: **10.1039/B922733D**.
19 N. Wang, X. Li, Z. Tu, F. Zhao, J. He, Z. Guan, C. Huang, Y. Yi and Y. Li, Synthesis and electronic structure of boron-graphdiyne with an sp-hybridized carbon skeleton and its application in sodium storage, *Angew. Chem., Int. Ed.*, 2018, **57**, 3968–3973, DOI: **10.1002/anie.201800453**.
20 N. V. Rao Nulakani and V. Subramanian, *J. Phys. Chem. C*, 2016, **120**(28), 15153–15161, DOI: **10.1021/acs.jpcc.6b03562**.
21 L. Zhao, P. Sang, S. Guo, X. Liu, J. Li, H. Zhu and W. Guo, Promising monolayer membranes for $CO_2/N_2/CH_4$ separation: Graphdiynes modified respectively with hydrogen, fluorine, and oxygen atoms, *Appl. Surf. Sci.*, 2017, **405**, 455–464, DOI: **10.1016/j.apsusc.2017.02.054**.
22 M. Bartolomei, E. Carmona-Novillo, M. I. Hernández, J. Campos-Martínez, F. Pirani and G. Giorgi, Graphdiyne pores: "Ad hoc" openings for helium separation applications, *J. Phys. Chem. C*, 2014, **118**, 29966–29972, DOI: **10.1021/jp510124e**.
23 E. García-Arroyo, J. Campos-Martínez, M. Bartolomei, F. Pirani and M. I. Hernández, Molecular hydrogen isotope separation by a graphdiyne membrane: a quantum-mechanical study, *Phys. Chem. Chem. Phys.*, 2022, **24**, 15840–15850, DOI: **10.1039/D2CP01044E**.
24 S. W. Cranford and M. J. Buehler, Selective hydrogen purification through graphdiyne under ambient temperature and pressure, *Nanoscale*, 2012, **4**, 4587–4593, DOI: **10.1039/C2NR30921A**.
25 K. Xu, N. Liao, M. Zhang and W. Xue, Atomic-scale investigations of enhanced hydrogen separation performance from doping boron and nitrogen in graphdiyne membrane, *Int. J. Hydrogen Energy*, 2020, **45**, 28893–28902, DOI: **10.1016/j.ijhydene.2020.07.174**.
26 Y. Jiao, A. Du, M. Hankel, Z. Zhu, V. Rudolph and S. C. Smith, Graphdiyne: a versatile nanomaterial for electronics and hydrogen purification, *Chem. Commun.*, 2011, **47**, 11843–11845, DOI: **10.1039/C1CC15129K**.
27 X. Zhang, R. Fang, D. Chen and G. Zhang, Using Pd-doped-graphyne to detect dissolved gases in transformer oil: A density functional theory investigation, *Nanomaterials*, 2019, **9**, 1490, DOI: **10.3390/nano9101490**.
28 Z. Meng, X. Zhang, Y. Zhang, H. Gao, Y. Wang, Q. Shi, D. Rao, Y. Liu, K. Deng and R. Lu, Graphdiyne as a high-efficiency membrane for separating oxygen from harmful gases: A first-principles study, *ACS Appl. Mater. Interfaces*, 2016, **8**, 28166–28170, DOI: **10.1021/acsami.6b08662**.
29 P. Rezaee and H. R. Naeij, A new approach to separate hydrogen from carbon dioxide using graphdiyne-like membrane, *Sci. Rep.*, 2020, **10**, 13549, DOI: **10.1038/s41598-020-69933-9**.
30 Y. B. Apriliyanto, N. Faginas Lago, A. Lombardi, S. Evangelisti, M. Bartolomei, T. Leininger and F. Pirani, Nanostructure selectivity for molecular adsorption and separation: the case of graphyne layers, *J. Phys. Chem. C*, 2018, **122**, 16195–16208, DOI: **10.1021/acs.jpcc.8b04960**.
31 H. Hamyali, F. Nosratinia, A. Rashidi and M. Ardjmand, Anthracite coal-derived activated carbon as an effectiveness adsorbent for superior gas adsorption and CO_2/N_2 and CO_2/CH_4 selectivity: Experimental and DFT study, *J. Environ. Chemical Engineering*, 2022, **10**, 107007, DOI: **10.1016/j.jece.2021.107007**.
32 S. Rafiq, Z. Man, A. Maulud, N. Muhammad and S. Maitra, Separation of CO_2 from CH_4 using polysulfone/polyimide silica nanocomposite membranes, *Sep. Purif. Technol.*, 2012, **90**, 162–172, DOI: **10.1016/j.seppur.2012.02.031**.
33 M. Rezakazemi, A. Ebadi Amooghin, M. M. Montazer-Rahmati, A. Fauzi Ismail and T. Matsuura, State-of-the-art membrane based CO_2 separation using mixed matrix membranes (MMMs): An overview on current status and future directions, *Prog. Polym. Sci.*, 2014, **39**, 817–861, DOI: **10.1016/j.progpolymsci.2014.01.003**.
34 N. M. Ismail, A. F. Ismail and A. Mustaffa, Characterization of polyethersulfone/cloisite 15A mixed matrix membrane for CO_2/CH_4 separation, *J. Teknol. Lab.*, 2014, **69**, 83–87, DOI: **10.11113/JT.V69.3402**.
35 A. Jamil, O. P. Ching and A. M. Shariff, Mixed matrix hollow fibre membrane comprising polyetherimide and modified montmorillonite with improved filler dispersion and CO_2/CH_4 separation performance, *Appl. Clay Sci.*, 2017, **143**, 115–124, DOI: **10.1016/j.clay.2017.03.017**.
36 D. S. Sholl and J. A. Steckel, *Density Functional Theory*, Wiley, Hoboken, 2009.
37 P. Giannozzi, S. Baroni, N. Bonini, M. Calandra, R. Car, C. Cavazzoni, D. Ceresoli, G. L. Chiarotti, M. Cococcioni and I. Dabo, *et al.*, QUANTUM ESPRESSO: a modular and open-source software project for quantum simulations of materials, *J. Phys.: Condens. Matter*, 2009, **21**, 395502, DOI: **10.1088/0953-8984/21/39/395502**.
38 **https://www.quantumespresso.org** (accessed 19 February 2024).

39 J. P. Perdew, K. Burke and M. Ernzerhof, Generalized gradient approximation made simple, *Phys. Rev. Lett.*, 1966, **77**, 3865–3868, DOI: **10.1103/PhysRevLett.77.3865**.

40 G. Kresse and D. Joubert, From ultrasoft pseudopotentials to the projector augmented wave method, *Phys. Rev. B: Condens. Matter Mater. Phys.*, 1999, **59**, 1758–1775, DOI: **10.1103/PhysRevB.59.1758**.

41 P. E. Blöchl, Projector augmented-wave method, *Phys. Rev. B: Condens. Matter Mater. Phys.*, 1994, **50**, 17953–17979, DOI: **10.1103/PhysRevB.50.17953**.

42 S. Grimme, J. Antony, S. Ehrlich and H. Krieg, A consistent and accurate ab initio parametrization of density functional dispersion correction (DFT-D) for the 94 elements H-Pu, *J. Chem. Phys.*, 2010, **132**, 154104, DOI: **10.1063/1.3382344**.

43 L. Goerigk, in *A comprehensive overview of the DFT-D3 London-dispersion correction*, ed. A. Otero de la Roza, and G. A. DiLabio, *Non-Covalent Interactions in Quantum Chemistry and Physics*, Elsevier, 2017, pp. 195–219, DOI: **10.1016/B978-0-12-809835-6.00007-4**.

44 I. Cabria, M. J. López and J. A. Alonso, Searching for DFT-based methods that include dispersion interactions to calculate the physisorption of H_2 on benzene and graphene, *J. Chem. Phys.*, 2017, **146**, 214104, DOI: **10.1063/1.4984106**.

45 H. J. Monkhorst and J. D. Pack, Special points for Brillouin-zone integrations, *Phys. Rev. B: Solid State*, 1976, **13**, 5188–5192, DOI: **10.1103/PhysRevB.13.5188**.

46 X. Gao, H. Liu, D. Wang and J. Zhang, Graphdiyne: synthesis, properties, and applications, *Chem. Soc. Rev.*, 2019, **48**, 908–936, DOI: **10.1039/C8CS00773J**.

47 Y. Du, W. Zhou, J. Gao, X. Pan and Y. Li, Fundament and application of graphdiyne in electrochemical energy, *Acc. Chem. Res.*, 2020, **53**, 459–469, DOI: **10.1021/acs.accounts.9b00558**.

48 A. Seif, M. J. López, A. Granja-DelRío, K. Azizi and J. A. Alonso, Adsorption and growth of palladium clusters on graphdiyne, *Phys. Chem. Chem. Phys.*, 2017, **19**, 19094–19102, DOI: **10.1039/C7CP03263C**.

49 E. German, J. Sandoval, A. Recio, A. Seif, J. A. Alonso and M. J. López, Supported metal nanohydrides for hydrogen storage, *Chem. Mater.*, 2023, **35**, 1134–1147, DOI: **10.1021/acs.chemmater.2c03106**.

50 E. Germán, A. Alvarez-Yenes, J. A. Alonso and M. J. López, Adsorption of transition metal clusters on Boron-graphdiyne, *Appl. Surf. Sci.*, 2021, **548**, 149270, DOI: **10.1016/j.apsusc.2021.149270**.

51 N. Osouleddini and S. F. Rastegar, DFT study of the CO_2 and CH_4 assisted adsorption on the surface of graphene, *J. Electron. Spectrosc. Relat. Phenom.*, 2019, **232**, 105–110, DOI: **10.1016/j.elspec.2018.11.006**.

52 B. C. Wood, S. Y. Bhide, D. Dutta, V. S. Kandagal, A. D. Pathak, S. N. Punnathanam, K. G. Ayappa and S. Narasimhan, Methane and carbon dioxide adsorption on edge-functionalized graphene: A comparative DFT study, *J. Chem. Phys.*, 2012, **137**, 054702, DOI: **10.1063/1.4736568**.

53 C. Thierfelder, M. Witte, S. Blankenburg, E. Rauls and W. G. Schmidt, Methane adsorption on graphene from first principles including dispersion interaction, *Surf. Sci.*, 2011, **605**, 746–749, DOI: **10.1016/j.susc.2011.01.012**.

54 M. D. Ganji, Theoretical study of the adsorption of CO_2 on tungsten carbide nanotubes, *Phys. Lett. A*, 2008, **372**, 3277–3282, DOI: **10.1016/j.physleta.2008.01.032**.

55 P. Sang, L. Zhao, J. Xu, Z. Shi, S. Guo, Y. Yu, H. Zhu, Z. Yan and W. Guo, Excellent membranes for hydrogen purification: Dumbbell-shaped porous-graphynes, *Int. J. Hydrogen Energy*, 2017, **42**, 5168–5176, DOI: **10.1016/j.ijhydene.2016.11.158**.

56 Y. F. Li, Z. Zhou, P. W. Shen and Z. F. Chen, Two-dimensional polyphenylene: experimentally available porous graphene as a hydrogen purification membrane, *Chem. Commun.*, 2010, **46**, 3672–3674, DOI: **10.1039/B926313F**.

57 M. Abramowitz and I. A. Stegun, *Handbook of Mathematical Functions*. Dover Publications, New York, 1972.

